IEICE TRANS. INF. & SYST., VOL.E96–D, NO.4 APRIL 2013

PAPER Special Section on Medical Imaging

Segmentation of Liver in Low-Contrast Images Using K-Means Clustering and Geodesic Active Contour Algorithms

Amir H. FORUZAN[†*], ***Nonmember***, **Yen-Wei CHEN**[†a)], ***Member***, **Reza A. ZOROOFI**[††], ***Nonmember***, **Akira FURUKAWA**[†††], **Yoshinobu SATO**[††††], ***Members***, **Masatoshi HORI**[††††], ***and*** **Noriyuki TOMIYAMA**[††††], ***Nonmembers***

SUMMARY In this paper, we present an algorithm to segment the liver in low-contrast CT images. As the first step of our algorithm, we define a search range for the liver boundary. Then, the EM algorithm is utilized to estimate parameters of a 'Gaussian Mixture' model that conforms to the intensity distribution of the liver. Using the statistical parameters of the intensity distribution, we introduce a new thresholding technique to classify image pixels. We assign a distance feature vectors to each pixel and segment the liver by a K-means clustering scheme. This initial boundary of the liver is conditioned by the Fourier transform. Then, a Geodesic Active Contour algorithm uses the boundaries to find the final surface. The novelty in our method is the proper selection and combination of sub-algorithms so as to find the border of an object in a low-contrast image. The number of parameters in the proposed method is low and the parameters have a low range of variations. We applied our method to 30 datasets including normal and abnormal cases of low-contrast/high-contrast images and it was extensively evaluated both quantitatively and qualitatively. Minimum of Dice similarity measures of the results is 0.89. Assessment of the results proves the potential of the proposed method for segmentation in low-contrast images.

key words: *liver segmentation, segmentation of low-contrast images, geodesic active contours, liver intensity distribution modeling*

1. Introduction

Detection of hepatic tumors, extraction of vascular structures, and determination of portal venous segments and subsegments are the crucial steps prior to any liver treatment planning. Due to large number of images in a dataset, we need to employ Computer Assisted Diagnosis systems to analyze the liver images [1].

Liver segmentation is considered as a challenging task because of large shape variations, non-homogenous textures of abnormal livers, and low-contrast CT images [2]. The majority of research on liver segmentation falls into one of the following categories: Statistical Shape Models (SSM) [3], [4], probabilistic atlases [5], [6], Active Contour (AC) methods [7], [8], and histogram-based approaches [9]–[11].

Both the SSM-based approaches and probabilistic atlas methods suffer from large variations of livers shape and intensity, inaccurate registration and improper detection of corresponding landmarks. In the case of low-contrast datasets, the boundaries of the liver which are found by the SSM methods leak into the nearby organs. Both the Parametric and the Geometric Active Contour methods extensively are dependent on image gradient which leads to oversegmentation in the case of a low-contrast image. For both methods, locating the initial contour near the final one is an important requirement. Intensity-based liver segmentation methods are usually relied on a simplified model for the intensity distribution of the liver. Therefore, they miss vessels and tumors in abnormal livers. The problem of leakage is found in these methods too.

We propose a new intensity-based algorithm which mainly addresses the problem of segmentation of the liver in low-contrast CT images. It is a revised version of our previously proposed algorithm [11] so that it may be applied to more datasets [11]. The core of the method is a novel thresholding technique which we call 'Narrow-Band Thresholding' (NBT) in this paper. It consists of an appropriate selection and combination of conventional techniques to find the boundary of liver in low-contrast CT datasets. It simulates the task of a physician to find the border of liver by available image-processing applications. The segmented liver is considered as an initial liver boundary which is later refined by the 'Geodesic Active Contour' algorithm. The rest of this paper is prepared as follows. The proposed method is explained in Sect. 2. Extensive evaluation of our method is presented in Sect. 3. Section 4 is devoted to the discussion of the results and Sect. 5 concludes the paper.

2. The Proposed Method

2.1 Overview

The proposed method is a combination of 2D and 3D algorithms. A novel 2D algorithm is developed to exploit a priori knowledge about the boundary of liver in the neighbouring slices. Thus, it copes with shape variations in both normal and abnormal livers. Furthermore, the 'Geodesic Active Contour' (GAC) method, a 3D algorithm, guarantees smoothness of the final result.

The first step of our method is preprocessing that in-

Manuscript received June 19, 2012.
Manuscript revised October 30, 2012.

[†]The authors are with College of Information Science and Engineering, Ritsumeikan University, Kusatsu-shi, 525–8577 Japan.
[††]The author is with College of Engineering, University of Tehran, Tehran, Iran.
[†††]The author is with the Department of Radiology, Shiga University of Medical Science, Otsu-shi, 520–2192 Japan.
[††††]The authors are with the Department of Radiology, Graduate School of Medicine, Osaka University, Suita-shi, 565–0871 Japan.
[*]Presently, with the Department of Biomedical Engineering, Engineering Faculty, Shahed University, Tehran, Iran.
a) E-mail: chen@is.ritsumei.ac.jp

DOI: 10.1587/transinf.E96.D.798

Copyright © 2013 The Institute of Electronics, Information and Communication Engineers

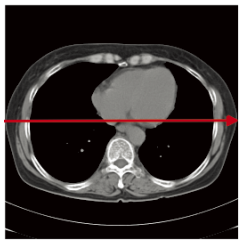

(a)

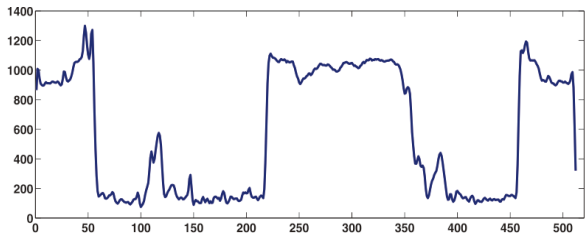

(b)

Fig. 1 Typical intensity profile of a middle row in liver CT images. (a) Direction of the profile. (b) Intensity variations.

cludes finding the bounding box of the abdominal region, extraction of the ribs and segmentation of a single slice by a physician. Next, we model the intensity distribution of the liver's tissue by a 'Dynamic Gaussian Mixture' using the initially segmented slice. Then, we apply the NBT method to segment the liver in the remaining slices. We find the volume of the liver through defining the borders of the liver in 2D slices. This volume is smoothed by the GAC algorithm and makes the final liver surface.

2.2 Preprocessing

As the first step of the preprocessing, we browse through the input CT volume to find a slice in which liver has a large cross-section. A doctor defines the border of the liver in this slice and this boundary is used as a priori knowledge in the next steps of our method.

To increase the speed of the code, we reduce the size of the input dataset by considering an ROI defined as the bounding box of the abdomen. We employ thresholding technique to extract the abdominal region. To define the proper threshold, we examine the intensity profile of the first axial slice of the input CT volume in the horizontal direction (Fig. 1). This slice which may contain heart, lungs, and liver is smoothed by a Gaussian filter. Then, the average of minimum and maximum of intensity in a middle row is chosen as the desired threshold. After thresholding the image, the bounding box of the abdomen is found and the input volume is resized so as to include only the abdomen region. The result is an average reduction of 30% in the size of a typical dataset.

We use the manually segmented slice for statistical analysis too. In this case, due to the existence of a large number of the liver pixels, estimation of the statistical parameters may be trustable. Since liver is a concrete volume, we follow the border of the liver in this slice in order to segment the liver in next slices and not to miss any separate part of the liver.

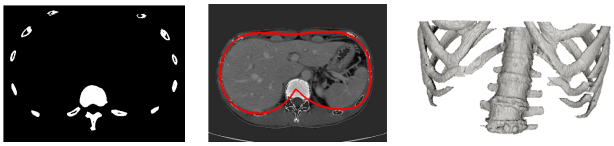

(a) (b) (c)

Fig. 2 Extraction of the ribs. (a) Segmented bones in a typical slice. (b) Fitting a spline to the centroid of the ribs. (c) 3D visualization of the extracted ribs.

The next step of the preprocessing is to remove the intercostal muscles that reside between the ribs and have the same intensity as the liver. They are removed by extraction of the ribs as explained in [11]. The ribs are extracted by thresholding technique (Fig. 2 (a)). The appropriate threshold is the average of the liver's intensity and the maximum intensity of a slice. After extraction of the ribs, we find the centroid of the ribs and fit a spline curve into these points (Fig. 2 (b)). This curve is used as a mask to remove parts of the muscles that are in contact with the liver (Fig. 2 (b)).

2.3 Dynamic Mixture Model

As explained in Sect. 2.1, the manually segmented slice is used to estimate the statistical parameters of the liver's pixels. We employ a dynamic Gaussian mixture to model the intensity distribution of the liver. By dynamic, we mean that the number of components in the model is not fixed. Estimation of the parameters is done using the 'Expectation Maximization' (EM) algorithm. The EM algorithm consists of two steps: The E-step which estimates the posterior probability and the M-step which calculates the model parameters [13]. Given the initial parameters μ_k^0, Σ_k^0, π_k^0 and the obtained π_k^0, the t^{th} iteration of E-step and M-step can be implemented in Eq. (1) and Eq. (2), respectively.

$$\gamma^t(z_{nk}) = \frac{\pi_k^t N(X_n|\mu_k^t, \Sigma_k^t)}{\sum_{j=1}^K \pi_j^t N(X_n|\mu_j^t, \Sigma_j^t)}, \; N_k^t = \sum_{n=1}^N \gamma^t(z_{nk}). \tag{1}$$

$$\mu_k^{t+1} = \frac{1}{N_k} \sum_{n=1}^N \gamma^t(z_{nk}) X_n, \qquad \pi_k^{t+1} = \frac{N_k^t}{N},$$

$$\Sigma_k^{t+1} = \frac{1}{N_k^t} \sum_{n=1}^N \gamma^t(z_{nk})(X_n - \mu_k^{t+1})(X_n - \mu_k^{t+1})^T,$$

$$S.t. \qquad \sum_{k=1}^K \pi_k^{t+1} = 1. \tag{2}$$

In a Gaussian mixture model, K normal random variables $N(X|\mu_k^t, \Sigma_k^t)$, $1 \le k \le K$ are combined to produce a Gaussian mixture, where μ_k^t and Σ_k^t are the mean and the standard deviation of kth component for the t^{th} iteration. Each component shares π_k^t ($0 \le \pi_k \le 1$, $1 \le k \le K$) in the whole distribution. In Eq. (1), $\gamma^t(z_{nk})$ is the posterior probability corresponding to the kth component of the t^{th} iteration

and the sample X_n, N_k is the number of samples corresponding to the kth component, and N is the total number of the samples. In Eq. (2), the superscript $t+1$ means the iteration step of the parameters and the superscript T is the transpose operator. If the parameter π_k corresponding to a component is less than 0.05, we do not consider this component in the model. At the start of the segmentation, the model has one component. We increase the number of the components one by one until the similarity measure between the segmented liver in the previous slice and the current slice is more than 0.95.

2.4 The NBT Method

Thresholding techniques segment objects based on intensity levels [12]. In the case of low-contrast images, using thresholding techniques lead to either leakage to nearby tissues or imperfections in segmentation results.

In this paper, we propose a novel thresholding technique to segment objects in low-contrast images. The main assumption in this method is to know the approximate position of the object's boundary as a priori knowledge. Since we employ 2D techniques to segment the liver, we use the mask of the liver in the previous slice as a priori knowledge to define a search region for the border of the liver in the next slice. Assuming the inter-slice resolution of the input data is high enough, the boundary of the liver in the next slice does not go far from its border in the previous slice. The K-means clustering is used to decide on whether a pixel in the search region belongs to the liver or not.

The main steps of the NBT method are shown in Fig. 3. Assuming the cross-section of the liver in ith slice is divided into m parts and the boundary of the liver for each part ($Mask_{i,j}$, $1 \le j \le m$) is known, we define a search range ($SR_{i+1,j}$) corresponding to the part j in the $(i+1)$th slice, defined by Eq. (3).

$$SR_{i+1,j} = xor(Mask_{i,j} \oplus SE_{Dilation}, Mask_{i,j} \ominus SE_{Erosion}) \quad (3)$$

In Eq. (3), $Mask_{i,j}$ is the cross-section of the liver corresponding to the jth part in slice i. $SE_{Dilation}$ and $SE_{Erosion}$ are the structuring elements used for dilation and erosion, respectively. These elements were empirically selected to be disks with a radius of 2 pixels. Furthermore, *xor* is exclusive-or operator in Eq. (3). We search for the liver's border in the current slice in the region $SR_{i+1,j}$. This region is a narrow band around the boundary of the liver (as shown in Fig. 6 (a)).

Next, the EM algorithm estimates the statistical parameters of the liver's tissue slice-by-slice so as to follow minor variations in the parameters.

Then, we threshold the input image to find 'Candidate Pixels'. If the intensity model of the liver includes K Gaussian components and the parameters of the kth component ($1 \le k \le K$) are μ_k and σ_k, we threshold each component in the narrow region $[Th_{Lk}, Th_{Hk}]$ (defined in Eq. (4)) to find the Candidate Pixels

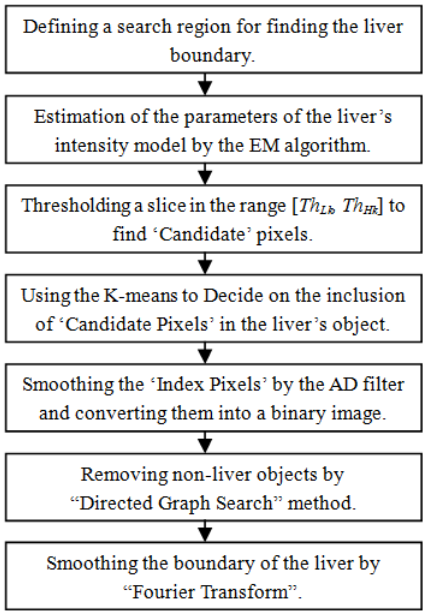

Fig. 3 The main steps of the NBT method.

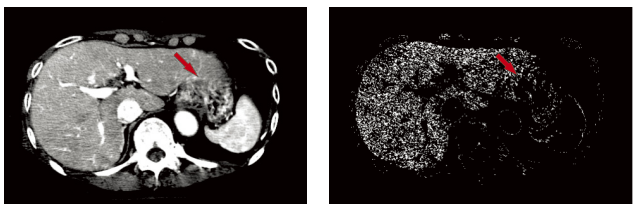

(a) (b)

Fig. 4 (a) Due to low-contrast between liver and the nearby tissues, boundary of the liver where it is shown by the red arrow cannot be defined clearly. (b) Thresolding in the narrow band around the liver's mean intensity helps in defining the border of the liver.

$$Th_{Lk} = \mu_k - BW_k,\ Th_{Hk} = \mu_k + BW_k,\ BW_k < 0.4\sigma_k. \quad (4)$$

BW_k is defined as a factor of σ_k ($BW_k = \beta.\sigma_k$, $\beta < 0.4$).

The output of this step is a large number of isolated pixels. The pixels of non-liver objects are scattered while the liver's pixels are grouped together (Fig. 4 (b)). We choose the parameter BW_k to be much less than $4\sigma_k$ ($BW_k < 0.4\sigma_k$). Thus, typical pixels of the liver are selected and the boundary of liver where is in contact with neighbouring tissues is defined. In the case of low-contrast datasets, we have to decrease β to prevent leakage into nearby tissues. Typical values for β are 0.15 and 0.3 corresponding to low-contrast and high-contrast datasets, respectively. Assuming a simple case where the intensity distribution of the liver is modeled by a single component $N(X|\mu_k, \Sigma_k)$. The area under the probability density function (S) is proportional to the number of liver pixels. The relationship between β and S is defined by Eq. (5).

$$S = \frac{1}{\sqrt{2\pi}\sigma_k} \int_{\mu_k-\beta\sigma_k}^{\mu_k+\beta\sigma_k} exp\Big(-\frac{(x-\mu_k)^2}{2\sigma_k^2}\Big).dx. \quad (5)$$

Numerical methods are used to calculate β for a spe-

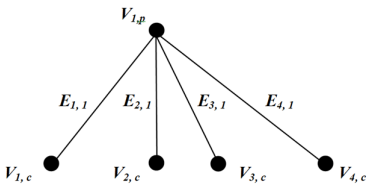

Fig. 5 Employing DGS to remove non-liver parts.

cific value of S. For example, if we want to keep 50% of the liver pixels by thresholding, β will be 0.711. We empirically found that the values of β are in the range [0.05 0.3] corresponding to very low-contrast to high-contrast datasets. In Fig. 4 (a), it is difficult to distinguish between the liver and the nearby tissues where shown by the red arrow. However, thresolding in the narrow band around the liver's mean intensity helps in defining the border of the liver (Fig. 4 (b)).

If a pixel is in the region defined by $Mask_{i,j} \ominus SE_{Erosion}$, it is considered as a liver pixel. For a pixel located in the search region, we use K-means clustering to determine if it belongs to the liver or not. We divide all pixels in the search region into far and near groups based on a distance transform feature. The pixels in the near group are assigned to the liver. At the end of this stage, the output of our algorithm is isolated liver pixels which we call them Index Pixels (Fig. 6 (c)).

To convert isolated 'Index Pixels' into a solid liver object, 'Anisotropic Diffusion Filter' is used to smooth the pixels and to avoid blurring of the boundary (Fig. 6 (d)) [14]. The smoothed image is normalized and thresholded by 0.5 to obtain a binary object (Fig. 6 (e)).

In the axial direction, if we browse through an abdominal CT dataset from the head towards the feet, the cross-section of the liver is divided into separated parts. In this step, we use 'Directed Graph Search' (DGS) to remove non-liver objects. In this technique, the connection of the livers cross-sections in the current slice and the previous slice are modeled by a directed graph G(N,E). The liver parts are modeled as the graph nodes (N) and the intersection of each part in the current slice and the previous slice are modeled as the graph edges. In Fig. 5, $V_{1,p}$ is a typical part of the liver in the previous slice, $V_{i,c}$ is the ith part of the liver in the current slice and $E_{i,j}$ is edge of the graph connecting $V_{i,c}$ and $V_{j,p}$. The edge $E_{i,j}$ is proportional to the intersection of $V_{i,c}$ and $V_{j,p}$ (Eq. (6)).

$$E_{i,j} = \frac{\left|V_{i,c} \cap V_{j,p}\right|}{\left|V_{j,p}\right|}. \tag{6}$$

An object with a relative intersection less than 50 is considered as a non-liver object.

The boundary of the liver found in this step is not smooth (Fig. 6 (e)). If the coordinates of the boundary points are analyzed by the Fourier transform, it will contain significant high-frequency components. The coordinates (x,y) are converted from spatial domain into frequency domain by Eq. (7).

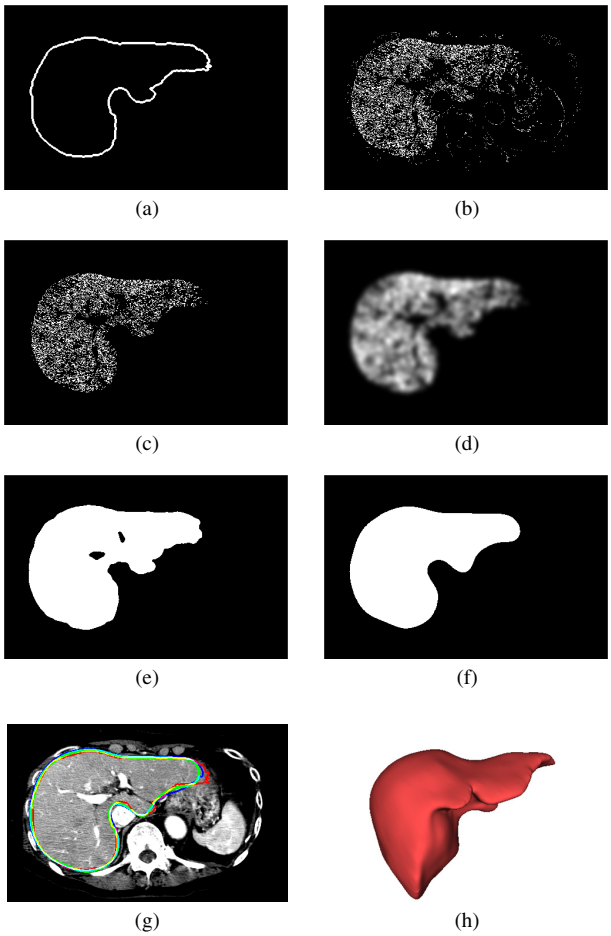

Fig. 6 Steps of the NBT method. (a) The search range of the liver's boundary, (b) 'Candidate Pixels' (c) 'Index Pixels' of the liver, (d) smoothing by the AD filter, (e) Thresholding the image of part (d), (f) Smoothing the boundary by the Fourier transform, (g) Comparison of initial (green), final (blue) and true liver border (red), (h) Smoothed surface of the liver by the GAC method.

$$F_x(k) = \sum_{j=1}^{N} x(j) e^{(\frac{-2\pi i}{N}(j-1)(k-1))}, \quad i = \sqrt{-1} \tag{7}$$

$$F_y(k) = \sum_{j=1}^{N} y(j) e^{(\frac{-2\pi i}{N}(j-1)(k-1))}.$$

In Eq. (7), N is the number of the boundary points which is usually greater than 100. If we remove high-frequency components, the boundary will be smooth. In the frequency domain, we keep only the first 15th components and, then, transfer them to spatial domain (Fig. 6 (f)) (Eq. (8)).

$$x(j) = \frac{1}{N} \sum_{k=1}^{15} F_x(k) e^{(\frac{+2\pi i}{N}(j-1)(k-1))}, \quad i = \sqrt{-1} \tag{8}$$

$$y(j) = \frac{1}{N} \sum_{k=1}^{15} F_y(k) e^{(\frac{+2\pi i}{N}(j-1)(k-1))}.$$

Visual inspections of the results reveal that smoothing the liver's border by this technique is significantly better

when compared to smoothing by conventional methods.

The initial surface of the liver is formed by integrating the liver's borders in 2D slices. The GAC algorithm is used for the evolution of the final surface (Fig. 6 (h)) [20]. To avoid leakage to nearby tissues, we empirically found it ideal to run the GAC algorithm for 30 to 40 iterations.

3. Results

We applied the proposed method to three different sets of the liver CT data including normal/abnormal, single/multi-phase, and low-contrast/high-contrast datasets. The first set belonged to Shiga University of Medical Science. We call it Group-I in this paper. It contained 10 normal datasets of low-contrast data with a resolution of $0.6836 \times 0.6836 \times 1\,\mathrm{mm}^3$ and a size of $512 \times 512 \times (185-263)$. The second set included 10 datasets of the second phase of abnormal livers. We call it Group-II in this paper. It was acquired by two GE scanners at Osaka University Hospital. The scanners were as follows: (1) LightSpeed QX/I, 4-channel MDCT (GE) with four detectors and (2) LightSpeed Ultra, 8-channel MDCT (GE) with eight detectors. Resolution of the images was $2.5 \times 2.5 \times 2.5\,\mathrm{mm}^3$ and $1.25 \times 1.25 \times 2.5\,\mathrm{mm}^3$ for LightSpeed QX/I and LightSpeed Ultra, respectively. The size of the datasets was $512 \times 512 \times 159$. Group-I and II contained 12-bit DICOM images. The third set was a public dataset belonged to the MICCAI 2007 Grand Challenge workshop [15]. Its specifications are given in [17]. In order to keep intensity information, we allocated 16-bit short integer variables to store pixel values. They were manually segmented by a physician and the segmentation results were used as ground truth. In the case of the MICCAI 2007 datasets, they were in Meta format with a pixel type of signed short integer. The evaluation was done by the authorities of the website and published there [17].

The proposed algorithm was mainly implemented in the MATLAB environment. However, we used the ITK toolkit for the GAC implementation and the VTK toolkit for 3D visualization of the results [18], [19]. The platform on which we ran the algorithm was an Intel®$Core^{TM}$ 2 Duo with 3 GBytes of RAM.

We extensively evaluated our method. In Table 1, quantitative evaluations by the metrics of the MICCAI 2007 Grand Challenge are shown [15]. The metrics are defined by mathematical expressions in Table 2.

In Table 2, d(x,y) is the Euclidean distance between the point x and y where x and y are the boundary points of the segmented volume by the proposed method and the manually segmented volume, respectively.

In Fig. 7, Dice similarity measure of the segmentation results corresponding to the Group-I and II are shown. Dice measure is introduced mathematically in Eq. (9).

$$S_{Dice} = \frac{2\left|M_{ref} \cap M_{auto}\right|}{\left|M_{ref}\right| + \left|M_{auto}\right|} \tag{9}$$

In Eq. (9), M_{ref} and M_{auto} refer to manually segmented volume and the segmented volume by the proposed method, respectively.

Table 1 Quantitative evaluation of the Group-I and II datasets.

Dataset	Signed Rel Vol Diff [%]	Avg Sym Surf Dist [mm]	Avg Sym RMS Surf Dist [mm]	Max Surf Dist [mm]	Vol Overlap Err [%]
Group-I	1.55	2.22	3.95	37.46	13.23
Group-II	4.06	1.88	3.04	22.27	12.51

Table 2 Mathematical expressions of the metrics used in Table 1.

Metric	Definition
$SignedRelVolDiff$	$\frac{Vol_{ref}-Vol_{auto}}{Vol_{ref}} \times 100$
$AvgSymSurfDist$	$\frac{\sum_{x\in M_{auto}} inf_{y\in M_{ref}} d(x,y)+\sum_{y\in M_{ref}} inf_{x\in M_{auto}} d(x,y)}{2}$
$AvgSymSurfDist$	$\sqrt{\frac{\sum_{x\in M_{auto}} inf_{y\in M_{ref}} d^2(x,y)+\sum_{y\in M_{ref}} inf_{x\in M_{auto}} d^2(x,y)}{2}}$
$Max\ Surf\ Dist$	$max\left(\max_{x\in M_{auto}}\left(inf_{y\in M_{ref}} d(x,y)\right)+\max_{y\in M_{ref}}\left(inf_{x\in M_{auto}} d(x,y)\right)\right)$
$VolOverlapErr$	$\left(1-\frac{\lvert M_{auto}\cap M_{ref}\rvert}{\lvert M_{auto}\cup M_{ref}\rvert}\times 100\right)$

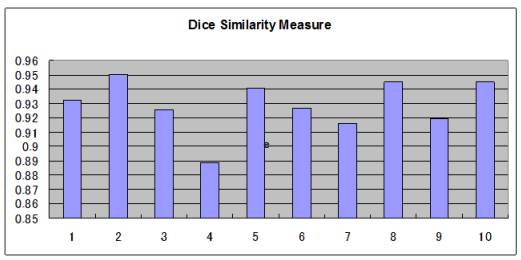

(a)

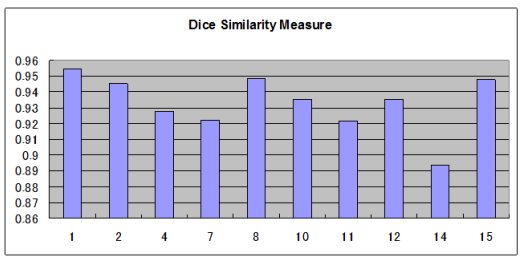

(b)

Fig. 7 Dice similarity measure for the (a) Group–I and (b) Group–II Datasets. X–axis is dataset number.

In order to compare our method with other researches, we registered the team RITS_UT (Ritsumeikan University - University of Tehran) in the MICCAI–2007 Grand Challenge and got the final score of 68.46 [17]. In Fig. 8, the results of the MICCAI-2007 Grand Challenge for three different cases are shown.

In Fig. 9, comparison of the segmentation results by the manual and the proposed method for four different slices are shown. The significance of the results of Fig. 9 is that the datasets of Fig. 9 (a) and (b) are low-contrast and those of

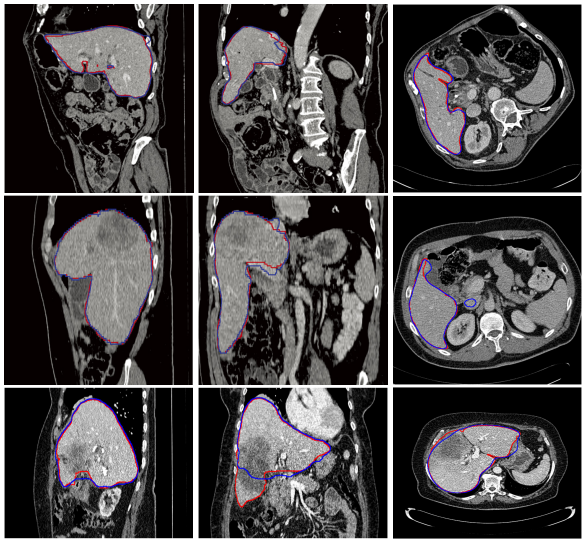

Fig. 8 From left to right, a sagital, coronal and transversal slice from a relatively easy case (1, top), an average case (4, middle), and a relatively difficult case (3, bottom). The outline of the reference and the proposed method segmentation results are in red and blue, respectively. Slices are displayed with a window of 400 and a level of 70.

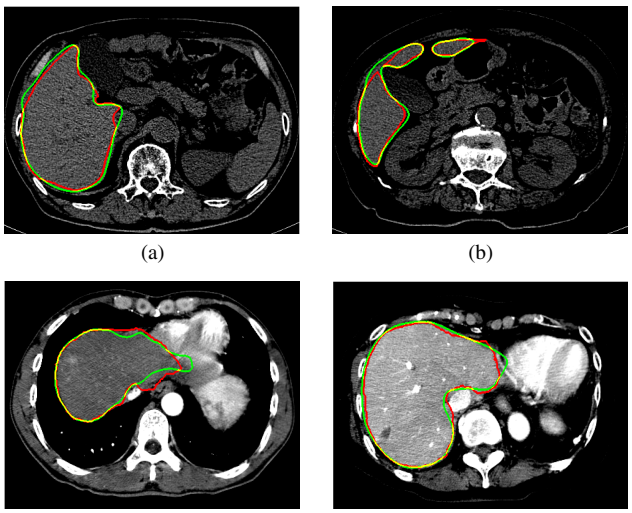

Fig. 9 Comparison of the manual segmentation (red) with the results of our method (green). Slices are displayed in an intensity range of [0 200]. (a), (b) Group–I, ID_1– no. 125 and ID_2–no. 111, respectively. (c), (d) Group–II, ID_4, no. 59. (d) ID_8, no. 132, respectively.

Fig. 9 (c) and (d) are abnormal livers.

In Fig. 10, surface rendering visualizations of three manually segmented datasets are compared with the results of our method.

In order to evaluate the effectiveness of the NBT method, we compared the results of our method with the results of both parametric and geometric Active Contours. In order to use several different metrics in the evaluation process, the comparison with region-based parametric Active Contours is performed by Dice similarity measure (Fig. 11) and the comparison with the Geometric Active Contours is

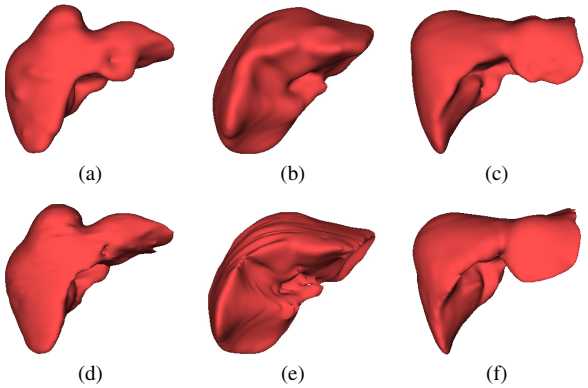

Fig. 10 Visualization of the segmented livers by our method (1st and 3rd row) and manual method (2nd and 4th row). Group-I: (a), (d) ID_1, (b), (e) ID_2, Group-II: (c), (f) ID_8.

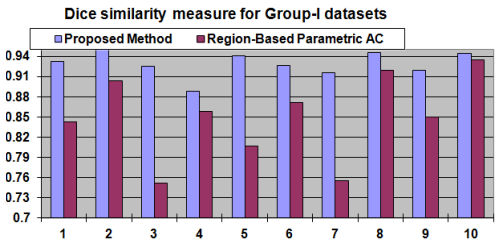

Fig. 11 Comparison of 'Region–Based Parametric Active Contours' with our method by Dice measure for Group–I datasets. X-axis is dataset number and Y–axis is Dice similarity measure.

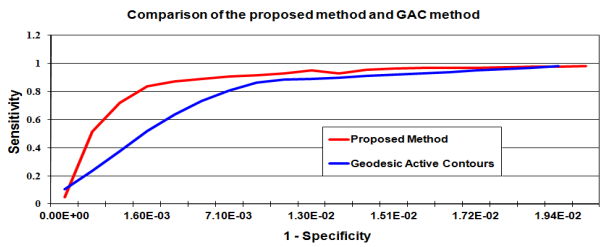

Fig. 12 ROC curve compares the results of the liver segmentation by our method and the 'Geodesic Active Contours'. Source: Group–I, ID_1.

Table 3 Quantitative evaluation of the Group–I and II datasets.

textbfMeasure	textbfDefinition
Sensitivity	True Positive / (True Positive + False Negative)
Specificity	True Negative / (True Negative + False Positive)

done by ROC curve (Fig. 12). In Fig. 12, the ROC curve corresponding to the GAC method was prepared by increasing number of iterations of the algorithm. The ROC curve corresponding to our method was prepared by increasing the size of the beta parameter in the narrow-band range to include more pixels in the segmentation results.

'Sensitivity' and 'Specificity' are defined in Table 3.

Sensitivity analysis of our method is performed by plotting the variations of Sensitivity and Specificity measures for different values of the BW (Fig. 13).

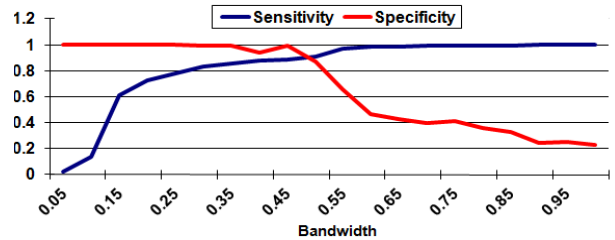

Fig. 13 Variations of Sensitivity and Specificity of the results for different values of BW (Bandwidth) parameter. Source: Group–II, ID_10.

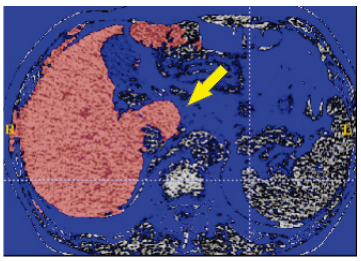

Fig. 14 The result of the liver segmentation for region-based snake leaked into the IVC (Note the yellow arrow). Source: Group–I, ID_04.

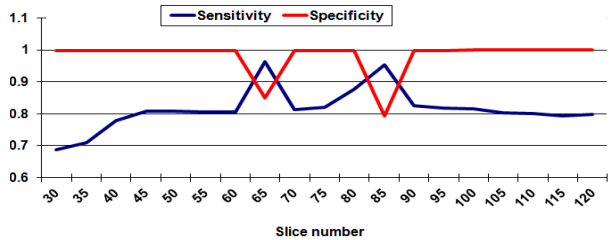

Fig. 15 Variations of Sensitivity and Specificity of the results for different values of BW (Bandwidth) parameter. Source: Group–II, ID_10.

Fig. 16 The vessels are missed in some cases in the segmentation results of our method. Source: Group–II, ID_08, no. 89

4. Discussion

In this paper, we introduced a new thresholding technique for the liver segmentation in low–contrast CT images. Thresholding was performed in a narrow range around the statistical mean of the intensity model. Our method is a concatenation of standard sub–algorithms. However, the proper selections and the order of the combinations of these sub–algorithms are so skillfully performed that our method had the potential to be applied to a diverse set of liver CT data including normal/abnormal and different phases of datasets.

Several diversities existed in the datasets which we used for evaluation: 1) The volumes included both normal and abnormal livers; 2) Some volumes were enhanced by contrast agent while some not; 3) The volume dimensions and the liver positions in the datasets substantially varied; 4) The inter–slice resolutions changed from 0.6 mm to 2.5 mm.

As can be seen in Fig. 9 (a) and (b), the intensity of the liver, colons, and ribs muscles are very similar. Thus, any conventional liver segmentation method will lead to extensive leakage to non-liver tissues. Minimum of Dice similarity measure for region–based snakes was as low as 0.75 (Fig. 11). However, the same measure for our method was more than 0.89. In Fig. 9 (c) and (d), while the result of the liver segmentation for region-based snake leaked into the IVC, our method excluded it from the segmentation result (Fig. 14).

Based on our previous experience [11], since the type and the number of the tissues neighbouring the liver vary significantly in the upper and lower slices, we used two different sets of parameters for the bandwidth (BW). In the upper slices, the liver is usually in contact with the ribs' muscles, stomach, and heart. However, the in lower slices; it may touch the colon, kidney, gallbladder, and ribs' muscles. Smoothing the initial boundary by the Fourier transform is another feature of our method which prevents leakage into nearby tissues, especially for small cross–sections of liver (Fig. 9 (b)).

An improvement in the proposed method is the detection and segmentation of small sections of the liver (Fig. 9 (b)). Our method typically segments five more slices in the lower slices and one to three more ones in the upper slices [20].

Even though the proposed method starts segmentation with a slice in which liver has a large cross-section, there is no need to exactly find the largest cross-section of the liver as the sensitivity analysis in Fig. 15 shows. Analysis of the plot of Fig. 15 reveals that the selection of the largest slice does not have great impact on the final result. As the future work of our research, we will try to segment the initial slice automatically.

A distinguished feature of our method is segmentation of abnormal liver datasets. The second phase of Group–II datasets together with several datasets of MICCAI-2007 datasets belong to abnormal cases which contain tumors (Fig. 8). The tumors are either of higher or lower intensities with respect to the intensity of the liver. For these cases, we selected a different set of parameters in our algorithm. The switching mechanism between the two sets of the parameters is done by user interaction. We intend to use an automatic mechanism to select the appropriate set of the parameters. The results of the segmentation of the MICCAI–2007 datasets (Fig. 8) clearly showed the capability of the proposed method for the segmentation of the liver in any deliberate dataset.

Regarding some high-contrast images of Group–II

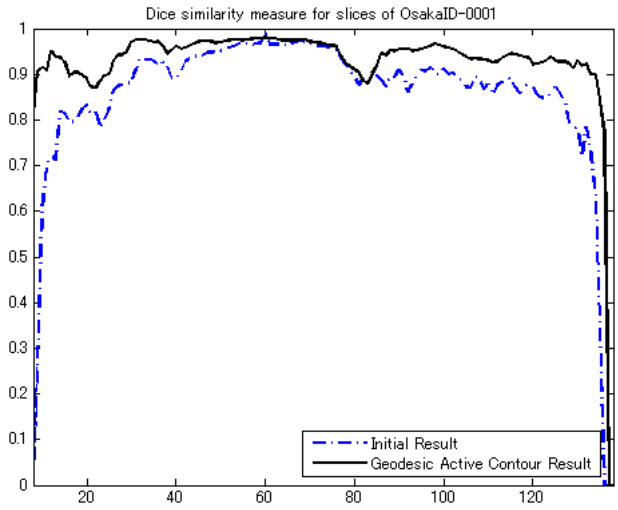

Fig. 17 The major contribution of the GAC algorithm to our method was towards segmentation of the upper–most and lower-most slices. Source: Group–II, ID_01

datasets, leakage occurred only in a single slice. In these cases, we did not consider the intensity range of vessels so as to prevent leakage to the IVC. However, the vessels were included in the segmentation results when the images were smoothed by the AD filters and the Fourier transform. In some cases, our method sometimes missed the vessels (Fig. 16).

The major contribution of the GAC algorithm to our method was towards segmentation of the upper–most and lower-most slices (i.e. the first and last slices in a volume) (Fig. 17). For the slices that were located in the middle of a dataset, the GAC did not change the results so much as the initial boundary was located near the final border. For some datasets, the results of the GAC algorithm led to over–segmentation since the image map for the evolution of active contour had no clear boundary for the liver.

The results in Fig. 10 revealed that the segmented livers by the proposed method considerably resembled the results of the manual segmentation. 3D visualization of segmented livers could potentially be used in the preoperative evaluation of the liver, too.

Another achievement of our method was the segmentation of the liver where there was Partial Volume Effect (PVE). The PVE is a source of ambiguity in defining borders of the tissues. However by using the proposed NBT technique, over-segmentation was prevented where there is the PVE (Fig. 9 (c), (d)).

The proposed method was a combination of 2D and 3D approaches. It exploited a priori information of the previously segmented slices, which was inherent in 2D segmentation methods, to tune the liver boundary for a variety of the liver shapes. It also took advantage of the smoothness of 3D approaches introduced by the 3D Active Contour algorithm.

Comparison of our method with the 'Geodesic Active Contour' performed by the ROC curve (Fig. 12) revealed that our method was superior to Active Contour method and

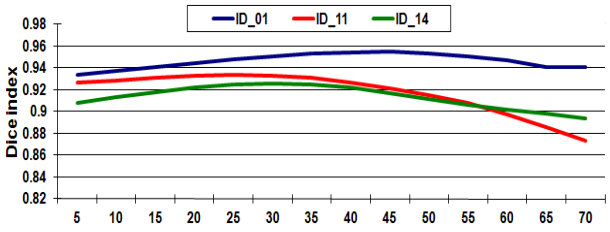

Fig. 18 Variations of Dice measure with respect to number of iterations of 'Geodesic Active Contour' for three sample datasets. Source: Group–II: blue, pink and green curves correspond to ID_1, ID_11 and ID_14, respectively.

led to higher true positive rates with lower false positive rates.

In order to improve our method and get better results, we have to exploit a priori information of the previously segmented slice more significantly and design a new image map for the Active Contour algorithm that resists leakage.

Segmentation of a dataset including 185–263 slices took 18–22 minutes. We plan to thoroughly implement our method in C++ environment and reduce the run-time to acceptable rates.

We analyzed the effect of the number of iterations of the GAC algorithm on the segmentation results for three sample datasets using Dice similarity measure (Fig. 18). As can be seen in Fig. 18, choosing a low or high number of iterations for the GAC algorithm results in reducing the Dice measure. Thus, it can be concluded that the optimum result is found if the number of iterations of the GAC algorithm is between 30 to 40. In Fig. 18, it can be concluded that the Active Contour algorithm needs acceptable initial surfaces as the input. This method also leaks to nearby tissues in the case of low–contrast images.

5. Conclusion and Future Works

In this paper, we presented an intensity–based algorithm to segment normal/abnormal livers in low/high–contrast and single/multi–phase CT datasets. The results of liver segmentation in MICCAI datasets gained a high score. In case of low–contrast images, our method outperformed the known techniques for object segmentation.

As the works for future, we plan to find and segment the initial slice automatically, find the boundary between the heart and the liver and design a surface mask for ribs.

Acknowledgments

This work was supported in part by the Grand–in Aid for Scientific Research from the Japanese Ministry for Education, Science, Culture and Sports under the Grand No. 21300070 and in part by the R–GIRO Research fund from Ritsumeikan University.

References

[1] Y. Nakayama, Q. Li, S. Katsuragawa, R. Ikeda, Y. Hiai, K. Awai,

et al., "Automated hepatic volumetry for living related liver transplantation at multisection CT," Radiology, vol.240, no.3, pp.743–748, 2006.
[2] P. Campadelli and E. Casiraghi, "Liver segmentation from CT scans: A survey," Lect. Notes Comput. Sci., 4578, pp.520–528, 2007.
[3] H. Ling, S.K. Zhou, Yefeng Zheng, B. Georgescu, M. Suehling, and D. Comaniciu, "Hierarchical, learning–based automatic liver segmentation," IEEE Conference on Computer Vision and Pattern Recognition, 2008, CVPR 2008, pp.1–8, 2008.
[4] Y. Song, A.J. Bulpitt, and K. Brodlie, "Liver segmentation using automatically defined patient specific B–Spline surface models," MICCAI 2009 London, pp.43–50, 2009.
[5] M.G. Linguraru, J.K. Sandberg, Z. Li, F. Shah, and R.M. Summers, "Automated segmentation and quantification of liver and spleen from CT images using normalized probabilistic atlases and enhancement estimation," Medical Physics, vol.37, no.2, pp.771–783, 2010.
[6] E.M. Van Rikxoort, Y. Arzhaeva, and B. Van Ginneken, "Automatic segmentation of the liver in computed tomography scans with voxel classification and atlas matching," in 3D Segmentation In The Clinic: A Grand Challenge, ed. T. Heimann, M. Styner, B. van Ginneken, pp.101–108, 2007.
[7] A. Wimmer, G. Soza, and J. Hornegger, "Two–stage semi-automatic organ segmentation framework using radial basis functions and level sets," Proc. MICCAI Workshop 3D Segmentation in the Clinic: A Grand Challenge, 2007.
[8] R.S. Alomari, S. Kompalli, and V. Chaudhary, "Segmentation of the liver from abdominal CT using Markov random field model and GVF snakes," Proc. 2008 International Conference on Complex, Intelligent and Software Intensive Systems, pp.293–298, 2008.
[9] A. Foruzan, R. Zoroofi, Y. Sato, M. Hori, T. Murakami, H. Nakamura, and S. Tamura, "Automated segmentation of liver from 3d CT images," Int. J. Computer Assisted Radiology and Surgery, vol.1, no.7, pp.71–73, 2006.
[10] M. Selver, A. Kocaoglu, G. Demir, H. Dogan, O. Dicle, and C. Gzelis, "Patient oriented and robust automatic liver segmentation for pre–evaluation of liver transplantation," Computers in Biology and Medicine, vol.38, no.7, pp.765–784, 2008.
[11] A.H. Foruzan, R.A. Zoroofi, M. Hori, and Y. Sato, "A knowledge–based technique for liver segmentation in CT data," Computerized Medical Imaging and Graphics, vol.33, no.8, pp.567–587, 2009.
[12] M. Sezgin and B. Sankur, "Survey over image thresholding techniques and quantitative performance evaluation," J. Electronic Imaging, vol.13, no.1, pp.146–168, 2004.
[13] C.M. Bishop, Pattern Recognition and Machine Learning, Springer, 2006.
[14] P. Perona and J. Malik, "Scale–space and edge detection using anisotropic diffusion," IEEE Trans. Pattern Anal. Mach. Intell., vol.12, no.7, pp.629–639, 1990.
[15] B.V. Ginneken, T. Heimann, and M.A. Styner, "3D segmentation in the clinic: a grand challenge," Workshop on 3D segmentation in the clinic, MICCAI 2007, pp.7–15, 2007.
[16] V. Caselles, R. Kimmel, and G. Sapiro, "Geodesic active contours," Int. J. Comput. Vis., vol.22, no.1, pp.61–97, 1997.
[17] Available at: http://www.sliver07.org
[18] Available at: http://www.itk.org
[19] Available at: http://www.vtk.org
[20] A.H. Foruzan, Y.W. Chen, R.A. Zoroofi, A. Furukawa, Y. Sato, and M. Hori, "Segmentation of liver in low–contrast Images using K–means clustering and a priori knowledge," IEICE Technical Report, IE2009-27, 2009.

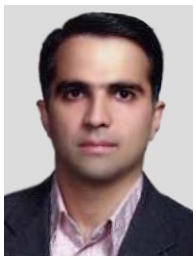

Amir Hossein Foruzan received the B.S. degree in Electronic Engineering from Sharif University of Technology, Iran, and the M.S. and Ph.D. degree in Biomedical Engineering from Tehran University, Iran. He received the Ph.D. degree in Biomedical Engineering from Tehran University, Iran in October 2010. From November 2008 to March 2010, he was a researcher at Intelligent Image Processing Laboratory, College of Information Science and Engineering, Ritsumeikan University.

(aforuzan@ece.ut.ac.ir)

Yen-Wei Chen received a B.E. degree in 1985 from Kobe Univ., Kobe, Japan, a M.E. degree in 1987, and a D.E. degree in 1990, both from Osaka Univ., Osaka, Japan. From 1991 to 1994, he was a research fellow with the Institute of Laser Technology, Osaka. From Oct. 1994 to Mar. 2004, he was an associate Professor and a professor with the Department of Electrical and Electronic Engineering, Univ. of the Ryukyus, Okinawa, Japan. He is currently a professor with the college of Information Science and Engineering, Ritsumeikan University, Kyoto, Japan. He was a visiting professor with the Oxford University, Oxford, UK in 2003 and a visiting professor with the Pennsylvania State University, USA in 2010. He is an Overseas Assessor of Chinese Academy of Science and Technology. He is an associate Editor of International Journal of Image and Graphics (IJIG) and editorial board members of the International Journal of Knowledge-based and Intelligent Engineering Systems and the International Journal of Information. His research interests include pattern recognition, image processing and radiological imaging. He has published more than 200 research papers in these fields.

Reza Aghaeizadeh Zoroofi received the B.S. degree in Electronic Engineering from Amir-Kabir University, Tehran, Iran, the M.S. degree in Telecommunication Engineering from Khajeh Nassir University, Tehran, Iran, and the Ph.D. degree in Medical Science from Osaka University, Osaka, Japan, in 1989, 1991, and 1998, respectively. From January to March 1997, he was a NEDO Researcher at Mechanical Engineering Laboratory, Ministry of International Trade and Industry, Tsukuba, Japan. From April 1997 to March 1998, he was a Research Fellow at the National Cardio-Vascular Center Research Institute, Osaka. From April 1998 to March 2000, he was a JSPS Postdoctoral Fellow in the Division of Functional Diagnostic Imaging, Osaka University Medical School. In April 2000, Dr. Zoroofi joined the School of Electrical and Computer Engineering, Faculty of Engineering, University of Tehran, Iran where he is currently working as an Associate Professor. In summers 2000 to 2007, Dr. Zoroofi collaborated at Osaka University Medical School as Invited Research Scholar and Invited Associate Professor. His research activities include works in the fields of medical image analysis and medical software development.

Akira Furukawa received a M.D. degree in 1984 and a PhD. degree in Medicine in 1997 from Shiga University of Medical Science Otsu, Japan. He was a resident doctor from 1994 to 1986 and was an assistant Professor of Shiga University of Medical Science from 1986 to 1993, and he served as a chief of Radiology Department in Saiseikai Noe Hospital in Osaka, Japan from 1993 to 1997. He was an assistant Professor from 1997 to 2000, and was a senior assistant Professor of Shiga University of Medical Science from 2000 to 2007. He is currently an associate Professor of Shiga University of Medical Science. He visited and served as a research fellow in Radiology Department of Long Island Jewish Medical Center for Albert Einstein school of Medicine in New York, USA from 1995 to 1997. He is an executive board member of Japanese Collage of Radiology, the Japanese Society of Interventional Radiology, and Japanese Society of Emergency Radiology. His research interests include Diagnostic Radiology, especially in Abdominal Radiology, Gastrointestinal Radiology, Emergency Radiology and Interventional Radiology. He has published more than 150 research papers and review articles in these fields.

Yoshinobu Sato received his B.S., M.S. and PhD degrees in Information and Computer Sciences from Osaka University, Japan in 1982, 1984, 1988 respectively. From 1988 to 1992, he was a Research Engineer at the NTT Human Interface Laboratories. In 1992, he joined the Division of Functional Diagnostic Imaging of Osaka University Medical School as a faculty member. From 1996 to 1997, he was a Research Fellow in the Surgical Planning Laboratory, Harvard Medical School and Brigham and Women's Hospital. He is currently an Associate Professor at Osaka University Graduate School of Medicine and an Adjunct Associate Professor at Graduate School of Information Science and Technology, Osaka University. His research interests include medical image analysis, computer assisted surgery, and computational anatomy. Dr. Sato is a member of IEEE, MICCAI, and CAOS-International, and an editorial board member of Medical Image Analysis and the International Journal of Computer Assisted Radiology and Surgery.

Masatoshi Hori received the B.S. and M.S. degrees in electrical engineering from Osaka University, Osaka, Japan in 1986 and 1988, respectively. Then he received the M.D. degree and the Ph.D. degree in medicine from Osaka University in 1994 and 2001, respectively. He is currently an Assistant Professor in the Department of Radiology, Osaka University Graduate School of Medicine. His research interests include diagnostic radiology, image analysis, and computer aided diagnosis. Dr. Hori is a member of Japanese Radiological Society, Japanese Society of Magnetic Resonance Imaging, Japanese Society of Angiography and Interventional Radiology, International Society of Magnetic Resonance in Medicine, and Radiological Society of North America.

Noriyuki Tomiyama received his M.S. and PhD degrees in Medicine and Radiology from Osaka University, Japan in 1987, 1993 respectively. From 1997 to 1999, he was an assistant professor in the Dept. of Radiology, Osaka University School of Medicine. In 1999, he was a research fellow in the Dept. of Radiology of Vancouver General Hospital, Canada. From 2000 to 2002, he was a staff in the Dept. of Radiology, Ehime National Hospital. From 2002 to 2006, he joined the Dept. of Radiology of Osaka University School of Medicine as an associate professor. From 2006 to 2010, he was an associate professor and Vice Chairman in Dept. of Radiology, Osaka University Graduate School of Medicine. He is currently a professor and Chairman in the Dept. of Radiology, Osaka University Graduate School of Medicine. He is a member of the board of directors of Japan Radiological Society.